Cellular and Molecular Life Sciences (2023) 80:129
https://doi.org/10.1007/s00018-023-04778-9

ORIGINAL ARTICLE

A neuroprotective role of Ufmylation through Atg9 in the aging brain of *Drosophila*

Huifang Li[1] · Zhenghong Yu[2] · Zikang Niu[1] · Yun Cheng[3] · Zhenhao Wei[1] · Yafei Cai[1] · Fei Ma[4] · Lanxin Hu[1] · Jiejie Zhu[1] · Wei Zhang[1]

Received: 28 February 2023 / Revised: 9 April 2023 / Accepted: 11 April 2023 / Published online: 22 April 2023

Abstract

Ufmylation is a recently identified small ubiquitin-like modification, whose biological function and relevant cellular targets are poorly understood. Here we present evidence of a neuroprotective role for Ufmylation involving Autophagy-related gene 9 (Atg9) during *Drosophila* aging. The Ufm1 system ensures the health of aged neurons via Atg9 by coordinating autophagy and mTORC1, and maintaining mitochondrial homeostasis and JNK (c-Jun N-terminal kinase) activity. Neuron-specific expression of Atg9 suppresses the age-associated movement defect and lethality caused by loss of Ufmylation. Furthermore, Atg9 is identified as a conserved target of Ufm1 conjugation mediated by Ddrgk1, a critical regulator of Ufmylation. Mammalian Ddrgk1 was shown to be indispensable for the stability of endogenous Atg9A protein in mouse embryonic fibroblast (MEF) cells. Taken together, our findings might have important implications for neurodegenerative diseases in mammals.

Keywords Uba5 · Ufl1 · Life span · Patj · Oxidative stress · Puc

Introduction

Autophagy is a conserved lysosomal clearance process whereby unneeded intracellular substances are packaged, degraded and recycled for cell viability and homeostasis [1, 2]. Experimental results suggest that autophagy is neuroprotective in the aging brain because mature neurons face hurdles in preventing cellular waste from accumulating over a lifetime without the aid of cell division to dilute these burdens [3]. Changes in autophagy flux and lysosomal hydrolysis thereby have been implicated as potential causative factors of cell death in neurodegenerative disorders [4, 5].

A hallmark of autophagy is the formation of autophagosome, a double-membrane vesicle that initiates at the pre-autophagosomal structure or phagophore assembly site (PAS) to engulf cellular contents [6]. The autophagic pathway is highly controlled by a series of autophagy-related (Atg) proteins, among which Atg9 is the sole transmembrane protein essential for autophagosome formation [7, 8]. Different from other Atg proteins, either diffuse in the cytosol, or present at the PAS, Atg9 has a unique and dynamic distribution by forming multiple punctate structures [9]. In yeast, Atg9-containing vesicles are derived from the Golgi apparatus and cycles between the cytoplasmic membrane pool and the PAS. The Atg9 vesicles then are recruited to PAS during nutrient deprivation to ultimately become part of the autophagosomal outer membrane [10]. Similarly, mammalian Atg9 traffics between the trans-Golgi network, endosomal system, and plasma membrane under basal conditions, whereas it is translocated to autophagic membranes upon autophagy induction to fuse with the lysosome [11]. Moreover, yeast Atg9 has also been observed to localize proximal to the mitochondria, which, however, remains controversial

Huifang Li, Zhenghong Yu, Zikang Niu, Yun Cheng and Zhenhao Wei have contributed equally to this work.

✉ Wei Zhang
weizhang@njau.edu.cn

1 College of Animal Science and Technology, Nanjing Agricultural University, Nanjing 210095, China

2 Department of Rheumatology and Immunology, Jinling Hospital, Affiliated Hosptial of Medical School, Nanjing University, Nanjing 210002, China

3 Jiangsu Cancer Hospital, Jiangsu Institute of Cancer Research, The Affiliated Cancer Hospital of Nanjing Medical University, Nanjing 210009, China

4 College of Life Science, Nanjing Normal University, Nanjing 210023, China

due to the lack of supporting data from cultured mouse and human cells [12].

In addition to autophagy, evidence in *Drosophila* midgut also emerges that Atg9 can interact with PALS1-associated tight junction protein (Patj), which acts with Tsc2 to repress the activity of mechanistic target of rapamycin (mTOR) complex 1 (mTORC1) (Fig. 1a) [13]. The mTORC1 kinase is a key mediator of nutrient-dependent control of protein synthesis [14]. Well-characterized substrates of mTORC1 include 4EBP (eIF4E-binding protein) and S6K (ribosomal protein S6 kinase), which are involved in the initiation of cap-dependent translation of mRNA [15, 16]. This function of mTORC1 is required for synaptic plasticity and memory consolidation as altered protein translation has a vital role

◂**Fig. 1** Characterization of Ufmylation in the aging brain of adult *Drosophila*. **a** The Ufmylation system and Atg9 regulation shown in relation to the ER. **b** Ufmylation in the brains of young (3-day-old) and aged (30-day-old) w^{1118} control male flies. Conjugated and monomeric Ufm1 proteins are indicated by arrowheads. Anti-β-actin was used as loading control. **c** Histogram showing the normalized ratio to β-actin of total Ufm1 (T-Ufm1), conjugated Ufm1 (C-Ufm1) and monomeric Ufm1 (M-Ufm1) protein in young and aged fly brains. Data represent the average ± SD for 3 independent experiments. $*p<0.05$, $**p<0.01$. **d** Normalized mRNA levels of indicated genes measured by quantitative RT-PCR. RNA was isolated from above-mentioned young and aged w^{1118} male adult heads. RNA levels were normalized to *kinesin* mRNA. Data represent the average ± SD of 3 independent experiments. $*p<0.05$, $**p<0.01$. **e** Climbing assays show the percentage of flies that climbed > 5 cm in 30 s. *UAS-Ddrgk1*^{RNAi} (NIG) was expressed in neurons with the elav-Gal4 driver. "elav" denotes elav-Gal4/ + by crossing with w^{1118}. *ns* not significant, $***p<0.001$. **f** Adult lifespan calculated by day at 29 °C. Broken lines indicate the time points aged at 29 °C when climbing assays in (**e**) were performed. $n=200$ flies per genotype; Log-rank test, $p<0.001$. **g** Climbing assays for pan-neuronal expression of *UAS-Uba5*^{RNAi} and *UAS-Ufl1*^{RNAi}. *ns* not significant, $***p<0.001$. **h** Adult lifespan at 29 °C. Broken lines indicate the time points when climbing assays in (**g**) were performed. $n=200$ flies per genotype; Log-rank test, $p<0.001$. **i** Left panel: TUNEL staining in aged (21-day-old) brains. elav-Gal4 was used to drive UAS-RNAi transgene for Ddrgk1. Cell apoptosis was indicated by fragmented DNA as labeled by TUNEL in red. Nuclei were labeled with DAPI (blue). Right panel: normalized ratio of TUNEL dots in each brain ($n\geq6$). $***p<0.001$. **j** Left panel: neuropil vacuolization (arrowhead) in hematoxylin and eosin-stained brain sections of aged (21-day-old) flies. Right panel: quantification of vacuoles in each brain ($n\geq7$). $**p<0.01$

in memory and cognitive decline [3, 17]. On the other hand, mTORC1 is also known as a negative regulator of autophagy in response to nutrient sensing. It phosphorylates Atg13 and transcription factor EB (TFEB) to block autophagosome formation and lysosome biogenesis [18, 19]. As a result, the interaction between Atg9 and Patj serves a second mechanism for Atg9 to regulate autophagy through antagonizing the mTORC1 signaling.

In this report, we provide evidence for a novel post-translational modification of Atg9 protein mediated via the Ufm1 (ubiquitin-fold modifier 1) conjugation system. Ufmylation is a recently identified ubiquitin-like modification catalyzed by the Ufm1-activating E1 enzyme (Uba5), Ufm1-conjugating E2 enzyme (Ufc1), and E3 ligase Ufl1 and its co-factor Ddrgk1, which is also known as Ufbp1 or C20orf116 (Fig. 1a) [20–22]. So far only limited Ufm1 substrates have been described, including Ddrgk1 itself, which anchors to the ER membrane and interacts with other target proteins through co-localizing with Ufl1 in a large protein complex [23–25]. Although Ufmylation previously has been connected to neurodevelopmental diseases and cancers, the substrates and underlying mechanisms are still largely unclear [26, 27]. Here we uncover an age-dependent decrease of the Ufmylation activity that is crucial for the nervous system function during the aging process of *Drosophila*. The Ufm1 conjugation system acts via Atg9 to regulate autophagy and mTORC1, and maintain mitochondrial homeostasis and JNK (c-Jun N-terminal kinase) activity in neuronal cells. The consequences of misregulation of Ufmylation in this context can be severe neurodegenerative conditions. Interestingly, a conserved Atg9 Ufmylation mediated by Ddrgk1 is affirmed in *Drosophila* neurons and mouse embryonic fibroblast (MEF) cells. The neuroprotective role of Ufm1, therefore, might have implications for degenerations, such as Parkinson's disease, Alzheimer's disease, and bovine spongiform encephalopathy in mammals.

Results

Deficiency in Ufmylation leads to age-progressive neurodegeneration

In *Drosophila* adult brain, we noticed an age-dependent reduction in the protein levels of total and covalent Ufm1, but not Ufm1 monomer, when monitoring Ufm1 expression using an antibody recognizing both conjugated and monomeric forms (Fig. 1b and c). Quantitative RT-PCR further revealed that the transcript levels of core components of the Ufm1 system were generally low in aged heads when compared to young ones (Fig. 1d). Taken together, the reduced activity of the pathway as a whole suggests a possible function of Ufmylation in the aging brain.

To explore this issue, we utilized the RNAi-mediated depletion of gene expression driven by elav-Gal4 in neurons. Flies carrying the Gal4 system were shifted to 29 °C after eclosion in order to enhance RNAi efficacy. Using this strategy, we tried to abrogate Ddrgk1 in adult brain, and relatively minimize its effect on neurodevelopment. Flies lacking Ddrgk1 in this setting by a UAS-RNAi from NIG-FLY, though exhibited a sharply reduced survival, were able to perform normally in a climbing assay at a young age, indicating limited influence from Gal4-UAS during the developmental phase (Fig. 1e and f). Nonetheless, a progressive locomotor defect was detected when these flies became old and impaired in their climbing ability (Fig. 1e). Thereafter, a new RNAi line against Ddrgk1 from VDRC KK collection was applied for the confirmation of the aging phenotype. The independent KK line showed a stronger Ddrgk1 knockdown efficacy as quantified by PCR (Supplemental Figure S1a). Owing to folded wings under elav-Gal4, flies with KK were drowned in food after emerging, leading to an early adult lethality. A Tub-Gal80^{ts} then was introduced to weaken the knockdown strength and enable normal development of KK adults, which mimicked the behavior of aged NIG flies when grew old (Supplemental Figure S1b and c). For the reason of convenience, the following analyses referring to Ddrgk1 hence were conducted based on the NIG stock. Similar trend

was also obtained when knocking down Uba5 and Ufl1 simultaneously in neurons using the same strategy (Fig. 1g and h), in that the impact on Ufmylation by silencing Uba5 or Ufl1 alone was much lower than the Ddrgk1 RNAi (Supplemental Figure S1d and e). Efficacy of the Uba5 and Ufl1 RNAi transgenes were verified by PCR (Supplemental Figure S1f and g). Attribution of aforementioned discoveries to genetic background, however, could be excluded because all UAS transgenes without Gal4 driver (UAS/+ by crossing with w^{1118}) behaved pretty well at an old age (Supplemental Figure S1h-o).

Shortened adult lifespan and movement disorder are features characteristic of *Drosophila* models of neurodegeneration [28]. To ask whether the phenotypes in Ufmylation deficiencies resulted from neurodegeneration, we documented apoptotic cell death using the TUNEL assay in aged brains. Indeed, knocking down Ddrgk1 in neurons showed a significant increase in TUNEL-positive signals, which was verified by depleting Uba5 and Ufl1 (Fig. 1i and Supplemental Figure S2a). Both flies also showed elevated vacuolization in aged brain by hematoxylin–eosin (HE) staining, while limited vacuoles were observed in their respective controls (Fig. 1j and Supplemental Figure S2b). These findings are suggestive of a neuroprotective role for Ufm1 conjugation system during the aging process.

Deficiency in Ufmylation leads to lysosomal–autophagic deficits

Dysfunction of the Ufm1 pathway is known to activate the ER stress response and lead to elevated expression of Bip chaperone and phosphorylation of eIF2α [29, 30]. Given ER stress is a main cause of neurodegenerative diseases, thus we first checked whether cells were stressed in the aging brain. Overall, there was an age-associated increase of ER stress in normal brains as indicated by unfolded protein response (UPR) of both Bip mRNA and eIF2α phosphorylation (Supplemental Figure S2c and e). This increase was more predominant in aged brains deprived of Uba5 and Ufl1, but not in Ddrgk1 RNAi when compared to control flies, although all flies suffered comparable levels of stress when they were young (Supplemental Figure S2c–e). The difference detected here is consistent with earlier findings that some pathway components may have function independent of Ufmylation [31]. On the other hand, it also appears unlikely that the neurodegeneration in our context is primarily regulated by ER stress.

In contrast, an abnormal lysosomal pathology was constantly observed with Ufmylation ablation when we stained the aged brains with acidotropic LysoTracker. As visualized with confocal microscopy, depleting Ufm1 machinery led to an aberrant lysosome accumulation, which was not seen in age-matched control counterpart (Fig. 2a–d). Given that normal lysosomes are required to fuse with autophagosomes to form autophagolysosomes in the process of autophagy [32], we next examined autophagy. LC3 is commonly considered as a good marker for studying autophagy. Upon autophagy, the cytosolic form of LC3, LC3-I, is converted to LC3-II, which is specifically targeted to the autophagosome membrane until fusion with lysosomes [33]. Western blot analysis demonstrated that the levels of LC3-I and LC3-II were relatively stable in control flies regardless of the age, while LC3-II accumulated merely in the aged heads with Ufmylation ablated, implying either an anomalous activation of autophagy with increased autophagosomal vesicles or an accelerated age-dependent stall in the autophagy flux in those flies (Fig. 2e and f). To distinguish the two possibilities, we evaluated the downstream effects of autophagic dysregulation by making use of an antibody against p62, a substrate for autophagic degradation [34]. In line with the latter, control flies constitutively degraded p62 in their heads, whereas aged but not young RNAi flies displayed an elevated level of p62, confirming a chronic block of autophagy caused by defects in the Ufm1 system (Fig. 2e and f).

A conserved Ufm1 modification of Atg9 mediated by Ddrgk1

In the Atg family regulating autophagy, Atg9 is the only transmembrane protein that must be synthesized and processed in the ER. In light of this, we asked whether Atg9 could interact with the Ufm1 E3 ligase complex containing Ddrgk1 on the ER membrane. Unfortunately, no interaction was recovered when affinity purification of Ddrgk1 was conducted from *Drosophila* S2 cells transfected to express both Ddrgk1 and Atg9 (Supplemental Figure S3a). Next, we also carried out a TurboID analysis of Ddrgk1-associated proteins in S2 cells. TurboID is based on the activity of a promiscuous BirA biotin ligase, which labels proteins that are in close proximity with the TurboID-tagged bait [35, 36]. This differs from affinity purification of protein complexes since it allows identification of highly transient interactions. Surprisingly, this strategy led to identification of Atg9 from biotin-cultured cells expressing TurboID-tagged Ddrgk1 after compared with the same cells expressing TurboID and biotin-free cells expressing Ddrgk1- TurboID (Fig. 3a and Supplemental Figure S3b). Then to further determine whether Atg9 could be Ufmylated, we purified Atg9-GFP from aged head of a UAS transgene driven by elav-Gal4, and analyzed Ufm1 covalence using the Ufm1 antibody. Western blot revealed that a conjugated Ufm1, with a molecular weight (~ 140 kDa) larger than Atg9-GFP, specially corresponded to the purified Atg9 protein, but was absent when Ddrgk1 was depleted (Fig. 3b). More interestingly, this transgene-directed expression of Atg9-GFP in the brain

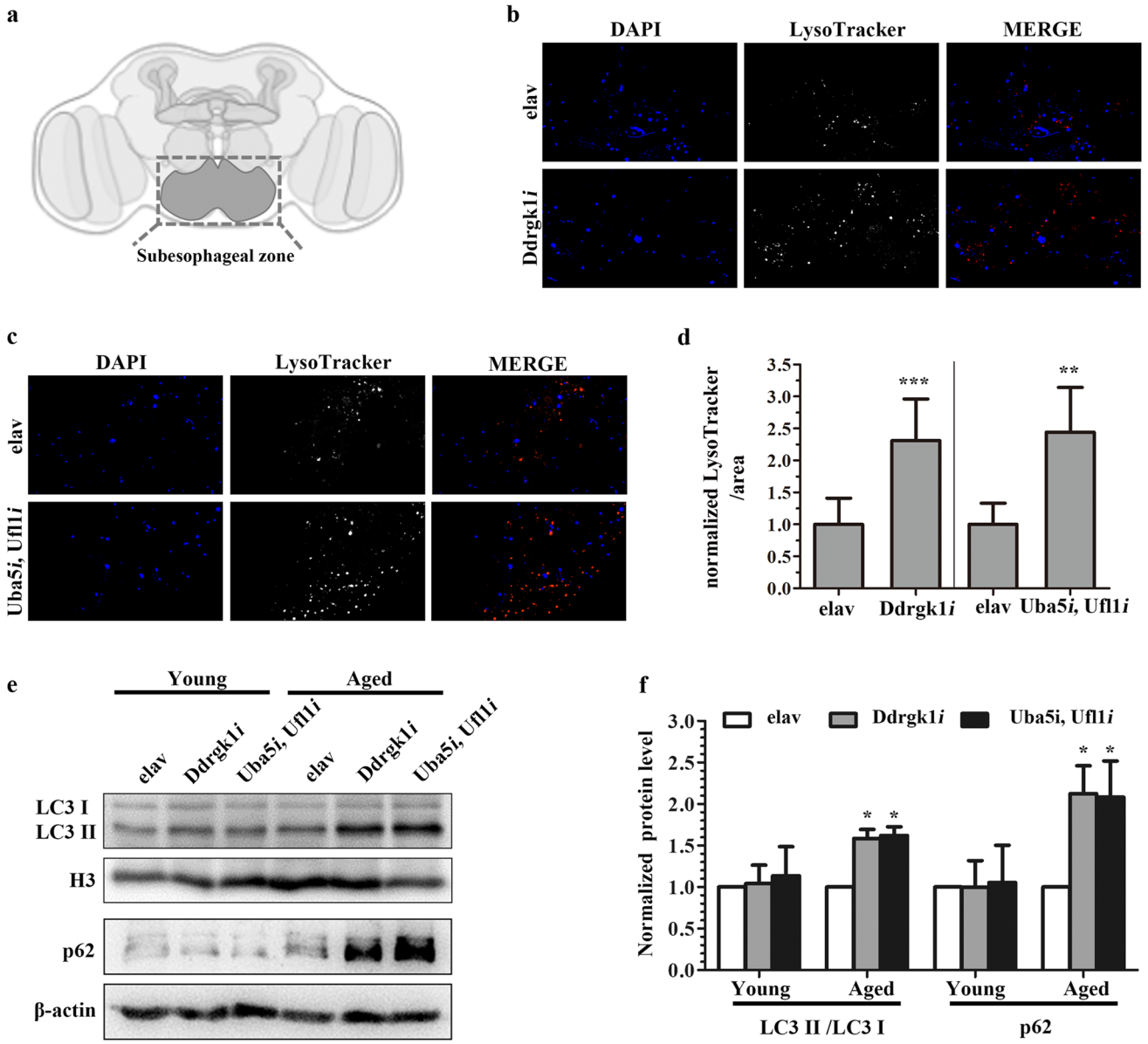

Fig. 2 Loss of Ufmylation led to lysosomal-autophagic deficits. **a** Diagram of a fly brain with the sub-esophageal zone highlighted. **b** Brains dissected from aged (21-day-old) elav-Gal4 control or Ddrgk1 knockdown flies were stained with LysoTracker Red. Images were captured from the same region of the sub-esophageal ganglion in each brain using the same microscope settings. DAPI was used to visualize nuclei (blue). **c** Brains dissected from aged (24-day-old) Uba5 and Ufl1 knockdown flies were stained with LysoTracker Red. Images were captured from the same region of the sub-esophageal ganglion. **d** LysoTracker probes above a uniform threshold were counted. Values represent average ± SD for $n \geq 7$ experiments with one control and one knockdown brain in each experiment. The normalized ratio between control and Ddrkg1 knockdown (left) is 1/2.31. $^{**}p < 0.01$, $^{***}p < 0.001$. **e** Immunoblots to visualize the levels of LC3 (LC3-I and LC3-II) and p62 in young (3-day-old) and aged (24-day-old) heads from flies expressing *UAS-Ddrgk1*^{RNAi} and *UAS-Uba5*^{RNAi}, *UAS-Ufl1*^{RNAi} under elav-Gal4 control. Antibody to H3 and β-actin were used as loading controls. **f** Histogram showing the normalized levels of LC3-II/LC3-I and p62 for representative lanes in (**e**). Data represent the average ± SD for 3 independent experiments. $^{*}p < 0.05$ when comparing to the control

was sensitive to the effect of Ddrgk1 modulation but with a refractory GFP transcript (Fig. 3c and Supplemental Figure S3c), hinting a post-transcriptional regulation of Atg9 in vivo by Ufmylation pathway. Considering Atg9 exists as highly motile vesicles, we conclude from these data that Ufm1 could modify Atg9 and sustain its expression, most likely through a transient interaction between Ddrgk1 and Atg9.

Drosophila possesses one Atg9, whereas mammals have Atg9A and Atg9B, among which Atg9A is ubiquitous but

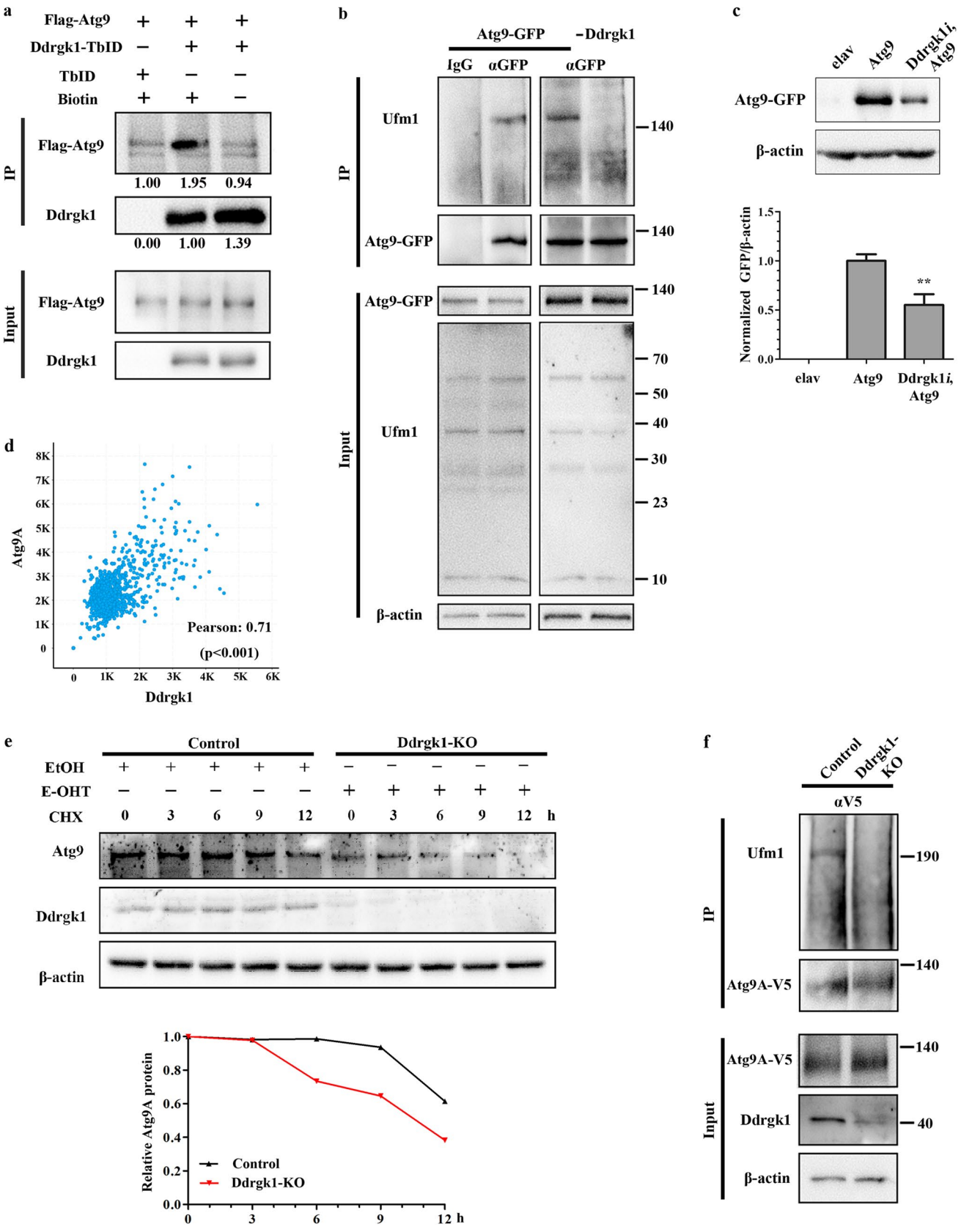
a
Flag-Atg9 + + +
Ddrgk1-TbID − + +
TbID + − −
Biotin + + −
IP
Flag-Atg9
1.00 1.95 0.94
Ddrgk1
0.00 1.00 1.39
Input
Flag-Atg9
Ddrgk1
b
Atg9-GFP −Ddrgk1
IgG αGFP αGFP
IP
Ufm1
Atg9-GFP
Input
Atg9-GFP
Ufm1
β-actin
140
70
50
40
30
23
10
c
elav
Atg9
Ddrgk1i, Atg9
Atg9-GFP
β-actin
Normalized GFP/β-actin
1.5
1.0
0.5
0.0
**
elav
Atg9
Ddrgk1i, Atg9
d
Atg9A
8K
7K
6K
5K
4K
3K
2K
1K
0
Pearson: 0.71
(p<0.001)
0 1K 2K 3K 4K 5K 6K
Ddrgk1
e
Control
Ddrgk1-KO
EtOH + + + + + − − − − −
E-OHT − − − − − + + + + +
CHX 0 3 6 9 12 0 3 6 9 12 h
Atg9
Ddrgk1
β-actin
Relative Atg9A protein
1.0
0.8
0.6
0.4
0.2
0.0
Control
Ddrgk1-KO
0 3 6 9 12 h
f
Control
Ddrgk1-KO
αV5
IP
Ufm1
Atg9A-V5
190
140
Input
Atg9A-V5
Ddrgk1
β-actin
140
40

◂**Fig. 3** Ddrgk1 mediates Atg9 Ufmylation and stabilizes its proteins. **a** Immunoblots to monitor the transient interaction between Ddrgk1-TurboID-V5 and Flag-Atg9. S2 cells were transfected to express TurboID-V5 or Ddrgk1-TurboID-V5 with Flag-Atg9. Cells were treated with biotin or water as a control (-) as indicated. Biotin-labeled proteins were recovered using Streptavidin beads, and blots were probed with anit-V5 and anti-Flag to visualize Ddrgk1 and bound Atg9. Relative protein levels were quantified and calculated for representative lanes. **b** Immunoblots to monitor Ufmylation of Atg9-GFP expressed under elav-Gal4 control in aged (21-day-old) fly heads. Left panel: Atg9-GFP proteins were recovered using GFP antibody raised in Alpaca, and blots were probed with anti-Ufm1 to visualize Ufmylation. Alpaca IgG was used as a control. Right panel: Atg9-GFP proteins were recovered from aged heads expressing *UAS-Ddrgk1*^{RNAi} under elav-Gal4 control. Anti-β-actin was used as loading control. **c** Immunoblots to visualize the level of GFP tagged Atg9 expressed in 21-day-old fly brains with and without Ddrgk1 depletion. Lower panel: histogram showing the normalized ratio of GFP/β-actin indicated for representative lanes in upper panel. Data represent 3 independent experiments. $^{**}p < 0.01$. **d** Correlation analysis of Ddrgk1 versus Atg9A in 7255 human samples from 6805 patients with tumors in CNS/brain using cBioPortal (www.cbioportal.org). Pearson correlation coefficient rho = 0.71 ($p < 0.001$). **e** Upper panel: immunoblots to visualize the levels of endogenous Atg9A and Ddrgk1 in MEF cells harvested from the Ddrgk1$^{F/F}$:ROSA26-CreERT2 mice. MEFs were treated with 4-OHT or ethanol to induce Ddrgk1 deletion or as a control. Before harvested, MEFs were pretreated with cycloheximide (CHX) for the indicated times. Anti-β-actin was used as loading control. Lower panel: histogram showing the quantification of Atg9A levels normalized to β-actin. **f** Immunoblots to monitor Ufmylation of Atg9A-V5. MEFs were treated with 4-OHT to induce Ddrgk1 deletion. Atg9A-V5 proteins were recovered using V5 antibody from MEFs transfected to express Atg9A-V5. Blot was probed with anti-Ufm1 to visualize Atg9A Ufmylation. Anti-β-actin was used as loading control

highly expressed in neurons of the central nervous system (CNS) [12]. By surveying samples from patients with tumors in CNS/brain using cBioPortal [37, 38], we noted a strong correlation between Ddrgk1 and Atg9A expression (Fig. 3d, but not Atg9B as per Supplemental Figure S3d), in keeping with the observation that low expression of Atg9 in aged fly head coincided with the diminished Ufm1 components (Fig. 1d). This persuaded us to get a more mechanistic understanding of the link between Ddrgk1 and Atg9A in mammals. As a first step, we tested the protein stability of Atg9A using a CHX (cycloheximide, inhibitor of protein synthesis) chase assay by taking advantage of a MEF cell lines harvested from the Ddrgk1$^{F/F}$:ROSA26-CreERT2 mice [39]. No surprise, Ddrgk1 was able to stabilize Atg9A proteins since endogenous Atg9A degraded faster when depletion of Ddrgk1 was induced by 4-hydroxytamoxifen (4-OHT) (Fig. 3e and Supplemental Figure S3e), in accordance with the regulation of Atg9 post-transcriptionally by Ddrgk1 in *Drosophila* (Fig. 3c and Supplemental Figure S3c). To follow up, we assessed the Ufmylation mediated by Ddrgk1 in those immortalized MEF cells by expressing a V5-tagged Atg9A. Results from V5 purification also showed an Ufm1-modified Atg9A that depended on the presence of Ddrgk1 (Fig. 3f). Intriguingly, the mammalian Atg9A seems to undergo a more complicated modification process as judging from the molecular weights of Ufmylated Atg9A (~ 190 kDa) and its fly ortholog (Fig. 3b and f).

The neuroprotective function of Ufmylation through Atg9

It is well established that Atg9 null mutant in *Drosophila* displays impaired developmental autophagy in larval stage [13]. To determine the function of Atg9 in adult brain, we again adopted the temperature sensitive RNAi driven by elav-Gal4, and found that loss of Atg9 selectively in neurons exhibited a reduced lifespan, characterized by a progressive climbing defect similar to Ufmylation disruption (Supplemental Figure S4a and b). RNAi efficacy of this Atg9 transgene was monitored by PCR (Supplemental Figure S4c). Nevertheless, over-expressing Atg9 by elav-Gal4 also led to a mild locomotor abnormality with age, showing the importance of fine-tuning autophagic activity in neurons, although the mortality of these flies was not severely affected (Supplemental Figure S4d and e). Likewise, attribution of abovementioned phenomena to UAS background turned up unlikely (Supplemental Figure S4f–h). Even so, introducing Atg9 in Ddrgk1- or Uba5-depleted neurons improved the climbing ability of aged flies and extended their life expectancy, suggesting phenotypes associated with Ufmylation ablation were actually caused by interruption of Atg9 function (Fig. 4a–b and Supplemental Figure S4i–j). Furthermore, compared with Ddrgk1 knockdown alone, co-expressing Atg9 did not compete for Gal4 binding by the UAS-RNAi cassette as measured by Ddrgk1 transcripts (Supplemental Figure S4k), but alleviated the neurodegeneration in those aged brains by reducing cell apoptosis and neuropil vacuolization (Fig. 4c–e). These physiological changes correlated with the restore of autophagy flux as indicated by LysoTracker, LC3-II and p62, markers for lysosome and autophagy (Fig. 4f–i). Since silencing Ddrgk1 relying on Gal4-UAS will be a major approach for analyzing the downstream signaling, two UAS-GFPs with separate insertion sites were further applied to rule out the concern for titration of elav-Gal4 (Supplemental Figure S4l–o). Altogether, we demonstrated that the Ufm1 pathway could act via Atg9 to protect the nervous system in aging.

Deficiency in Ufmylation leads to altered mTORC1 activity through Atg9

Besides promoting autophagosome formation, *Drosophila* Atg9 can also regulate autophagy in the adult intestine through antagonizing mTORC1 signaling by interacting with Patj [13]. Consequently we asked whether deficiency in Ufmylation would also affect the activity of mTORC1 in

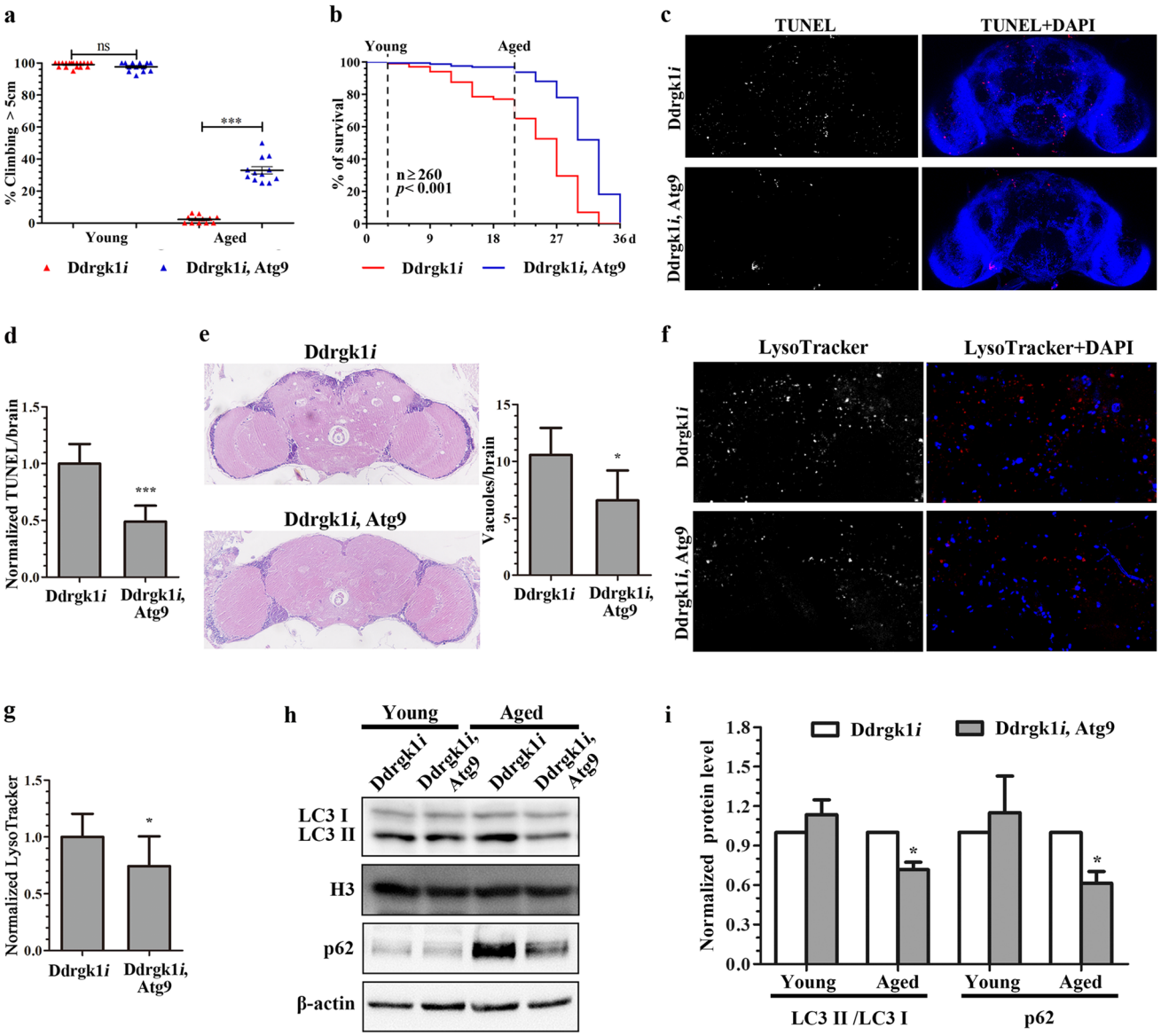

Fig. 4 Atg9 is involved in the neuroprotection of Ufmylation. **a** Climbing assay performed on Ddrgk1 knockdown and Atg9 co-expression flies under elav-Gal4 control. *ns* not significant, ***$p<0.001$. **b** Adult lifespan of Ddrgk1 knockdown flies calculated by day at 29 °C with and without co-expression of Atg9. $n\geq260$ flies per genotype; Log-rank test, $p<0.001$. **c** TUNEL staining in aged (21-day-old) brains of Ddrgk1 knockdown and Atg9 co-expression flies. Cell apoptosis was indicated by TUNEL in red and nuclei were labeled with DAPI in blue. **d** normalized ratio of TUNEL dots in each brain ($n\geq6$). ***$p<0.001$. **e** Left panel: neuropil vacuolization in HE-stained brain sections of aged (21-day-old) flies with denoted genotypes. Right panel: quantification of vacuoles in each brain ($n\geq6$). *$p<0.05$. **f** Aged (21-day-old) brains from Ddrgk1 knockdown flies with and without Atg9 co-expression were stained with LysoTracker Red. DAPI was used to visualize nuclei (blue). Images were captured from the same region of the sub-esophageal ganglion. **g** LysoTracker probes above a uniform threshold were counted. The normalized ratio is 1/0.74 for $n=7$ when comparing Ddrgk1 knockdown with Atg9 co-expression. *$p<0.05$. **h** Immunoblots to visualize the levels of LC3 and p62 in young (3-day-old) and aged (21-day-old) heads from Ddrgk1 knockdown flies with and without Atg9 co-expression. Antibody to H3 and β-actin were used as loading controls. **i** Histogram showing the normalized levels of LC3-II/LC3-I and p62 for representative lanes in (**h**). Data represent the average ± SD for 3 independent experiments. *$p<0.05$

flies. To address this question, we silenced the expression of Ddrgk1 and Ufl1 in S2 cells by dsRNA, both of which showed an increase in S6K phosphorylation (Fig. 5a), similar to Atg9 depletion under the same experimental setting (Supplemental Figure S5a and b). This connection between Ufmylation and mTORC1 was testified independently in adult eyes depleting Tsc1, a negative regulator of mTORC1 and tissue growth [40], since downregulating Ufm1 components by RNAi enhanced the Tsc1 loss-of-function phenotype by further enlarging eye size, but on its own had no

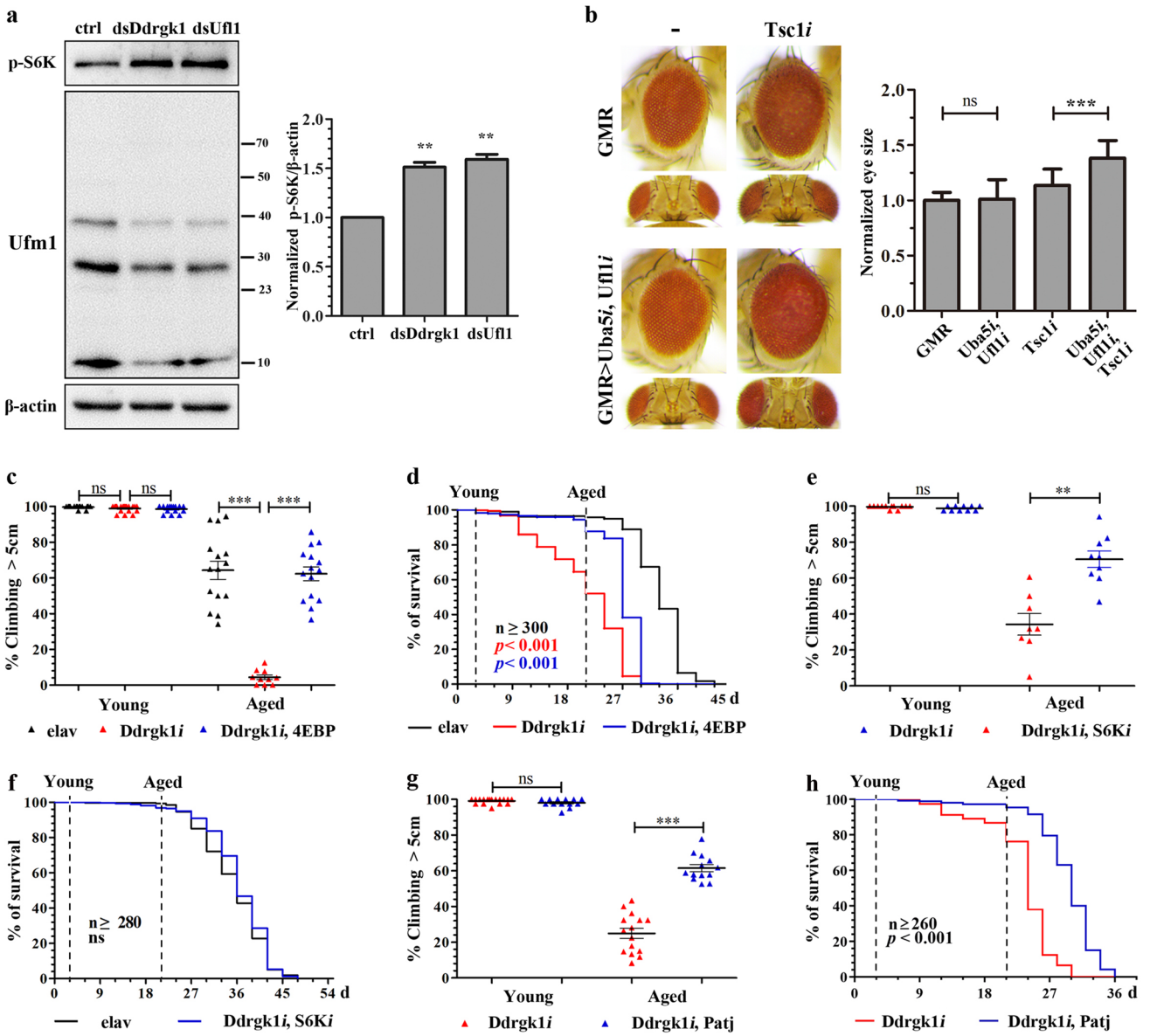

Fig. 5 Ufmylation acts via Atg9 to regulate mTORC1 activity. **a** Left panel: immunoblots to detect S6K phosphorylation. S2 cells were treated with dsRNA to deplete Ddrgk1 or Ufl1. Efficacy of Ddrgk1 or Ufl1 depletion was monitored indirectly by Ufm1 antibody. Anti-β-actin was used as loading control. Right panel: histogram showing the normalized ratio of p-S6K/β-actin indicated for representative lanes in left panel. Data represent 3 independent experiments. $^{**}p<0.01$. **b** Photomicrographs of adult eyes expressing GMR-Gal4 alone or with *UAS-Uba5*^{RNAi} and *UAS-Ufl1*^{RNAi}. Middle panel: co-expressed *UAS-Tsc1*^{RNAi}. Right panel: normalized eye size measured in pixels from digital images using ImageJ. Error bars indicate SD from measurement of at least 15 eyes for each genotype. *ns* not significant, $^{***}p<0.001$. **c** Climbing assay performed on Ddrgk1 knockdown and 4EBP co-expression flies under elav-Gal4 control; **e** Climbing assay performed on S6K^{RNAi} co-expression; **g** Climbing assay performed on Patj overexpression flies. *ns* not significant, $^{**}p<0.01$, $^{***}p<0.001$. **d** Adult lifespan of Ddrgk1 knockdown and 4EBP co-expression flies. $n\geq300$ flies; $p<0.001$ (in red) when comparing Ddrgk1 knockdown with elav-Gal4 control; $p<0.001$ (in blue) when comparing Ddrgk1 knockdown with 4EBP co-expression. **f** Adult lifespan by day at 29 °C. $n\geq280$ flies; *ns* not significant when comparing elav control with Ddrgk1 and S6K double knockdown. **h** Adult lifespan of Ddrgk1 knockdown flies with and without Patj overexpression. $n\geq260$ flies, $p<0.001$. Broken lines indicate the time points aged at 29 °C when climbing assays were performed

obvious eye phenotype (Fig. 5b). Efficacy of Tsc1 RNAi line was checked by PCR in Supplemental Figure S5c.

Then does mTORC1 also contribute to the neuroprotection of Ufm1 in the aging brain? Indeed, suppressing mTORC1 signaling by overexpressing 4EBP or depleting S6K ameliorated the survival deficit and movement disorder caused by Ufmylation ablation in neurons (Fig. 5c–f, efficiency of Ufmylation ablation was intact in the presence of

additional UAS cassette as estimated by Ddrgk1 transcripts in Supplemental Figure S4k), although high 4EBP and low S6K activities under normal conditions had opposite impacts on the adult lifespan, which apparently was independent of their genetic backgrounds (Supplemental Figure S5d–g). Efficacy of the S6K RNAi transgene was shown in Supplemental Figure S5h. In both human and *Drosophila* intestine, the multi-PDZ domain containing protein Patj interacts with Tsc2 to oppose the mTOR signaling, and Atg9, as outlined above, was known to act on mTORC1 through binding Patj [13]. To prove the involvement of Atg9, we managed to restore the climbing ability and life expectancy of Ddrgk1 RNAi flies via ectopically expressing Patj to inhibit mTORC1 by reinforcing the signal input from Atg9 (Fig. 5g and h, comparable Ddrgk1 transcripts in both brains were depicted in Supplemental Figure S4k), while expressing Patj by elav-Gal4 itself had subtle influence on aging (Supplemental Figure S4d and e). Conversely, silencing endogenous Patj in neurons displayed a marked trend toward neurodegeneration by assessing the survival and behavior of adult flies (Supplemental Figure S5i and j). Efficacy of the Patj depletion transgene was elucidated by PCR in Supplemental Figure S5k. In general, limited background effect was found for Patj flies in the absence of Gal4 (Supplemental Figure S4f–g and S5l). In sum, the altered mTORC1 activity supports a critical role of Atg9 in degenerative brains suffering from impaired Ufmylation.

Ufmylation regulates mitochondrial homeostasis and JNK through Atg9

Mitochondrial damages are profoundly implicated in neurodegenerative disease [41, 42]. It was noteworthy that a remarkable depletion of mitochondria was witnessed by MitoTracker staining when S2 cells were treated with dsRNA to silence Ddrgk1, Ufl1 or Atg9 (Fig. 6a and b). In aged but not young heads, ablating Ufmylation likewise compromised mitochondrial content as measured by the expressions of two mitochondrial components, COXIII and ATP5A [43, 44] (Fig. 6c–e), which could be revised by Atg9 overexpression (Fig. 6f–h), consistent with the idea that Atg9 acts downstream of Ufm1 machinery. Because a transversal feature of mitochondrial dysfunction is the alterations of oxidative metabolism [45], we also investigated the requirement of Ufmylation on the viability of adult fly in response to oxidative stress. In agreement with the mitochondrial abnormalities in aged flies, decreasing Uba5 and Ufl1 expressions in neurons resulted in increased sensitivity of young flies to H_2O_2, which was validated by an increase in the mortality of Ddrgk1-abolished flies under the same stress condition (Fig. 6i and j). Unexpectedly, co-expressing Atg9 this time only modestly rescued the elevated death rate caused by Ddrgk1 knockdown (Fig. 6k). This weak effect, however, could be potentiated via simultaneously supplementing mTORC1 inhibitor rapamycin into the fly medium containing H_2O_2, reflecting the involvement of both Atg9 and mTORC1 under oxidative stress (Fig. 6l).

An important amplification step subsequent to oxidative toxicity is activation of the JNK pathway that is known to prevent hosts against stress-induced damage and extend lifespan in *Drosophila* [46, 47]. Immunoblotting using anti-phospho-JNK antibody showed that young flies devoid of Ddrkg1 were deficient in JNK activation under oxidative stress, while overexpressing Atg9 did not further augment the phosphorylation level of JNK, likely masked by noise from non-neuronal tissues in the head (Fig. 7a). Yet, introducing Atg9 into neurons lacking Ddrgk1 upregulated the activity of JNK, hinting a rescue effect rendered by Atg9 (Fig. 7a). Puc is a transcriptional target of JNK signaling and encodes a phosphatase that inhibits JNK activity through a negative feedback mechanism [48]. Boosting JNK transduction by depleting Puc similarly exerted a small but functionally significant increase in the stress tolerance of the Ufm1-defective flies to H_2O_2 (Fig. 7b–d, efficiency of Ufmylation ablation was unchanged as per Supplemental Figure S4k). Accordingly, depriving Puc by elav-Gal4 on its own was insensitive to oxidative stress (Supplemental Figure S6a). Silencing Puc in neurons was also able to partially improve the locomotor ability and lifespan of these flies over time, which was true as well when one copy of the *Puc* gene was removed (Fig. 7e–h, performance of Puc RNAi and mutant alone is provided in Supplemental Figure S6b and c). Knockdown efficacy of the Puc transgene was judged by PCR in Supplemental Figure S6d. Hence, our study also conferred a physiological relevance of the JNK signaling pathway in the neuroprotection by Ufmylation.

Discussion

Although a genome-wide screen in human has found that genetic variants in components of the Ufm1 pathway are risk factors for Parkinson's disease, much less is known about the precise function of Ufm1 in the chronic neurological symptoms [49]. Here we aged *Drosophila* lifespan at 29 °C to accelerate the aging process, which might not be exactly the same as the physiological performance at the normal 25 °C. Nevertheless, our results illustrate a neuroprotective role of Ufmylation through Atg9 in the aging brain and head of *Drosophila* by assuming changes in head really reflect the brain in some scenarios. Failure of this regulation leads to age-progressive neurodegeneration, presumably reflected by a short survival accompanied with a locomotor dysfunction in aged but nut young flies. It is tempting to speculate that the degenerative phenotype observed here is due to ER stress response as the Ufm1 system is tightly related to the ER and

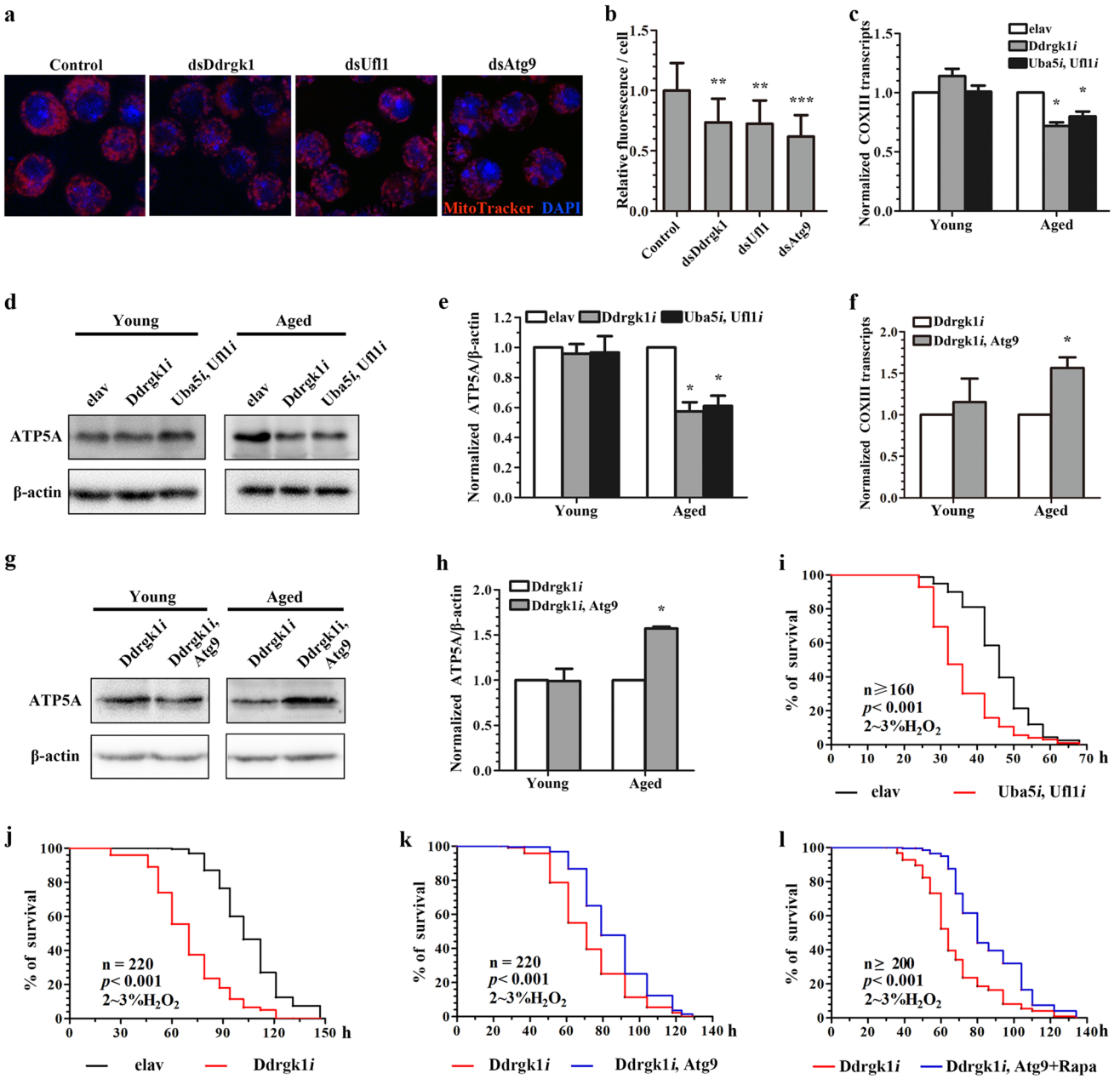

Fig. 6 Ufmylation acts via Atg9 to regulate mitochondrial homeostasis. **a** Visualization of active mitochondria by MitoTracker Red. S2 cells were treated with dsRNA to deplete Ddrgk1, Ufl1 or Atg9. DAPI was used to visualize nuclei (blue). **b** MitoTracker signals were measured as pixel intensity for each cell. Values represent average ± SD for $n = 50$ cells per treatment. $^{**}p < 0.01$, $^{***}p < 0.001$ comparing to the control. **c** Histogram showing the level of mitochondrial *COXIII* mRNAs measured by quantitative RT-PCR. Total RNA was extracted from young (3-day-old) and aged (24-day-old) fly heads with indicated genotypes under elav-Gal4 control. RNA levels were normalized to age-matched elav control after normalized to *kinesin* mRNA. Values represent average ± SD for 3 biological replicates. $^{*}p < 0.05$ when comparing to elav control. **d** Immunoblots to visualize the level of mitochondrial ATP5A in young (3-day-old) and aged (24-day-old) heads from flies of denoted genotypes. Anti-β-actin was used as loading control. **e** Histogram showing the normalized ratio of ATP5A/β-actin indicated for representative lanes in (**d**). Data represent 3 independent experiments. $^{*}p < 0.05$ when comparing to elav. **f** *COXIII* mRNAs measured by quantitative RT-PCR. Total RNA was extracted from young (3-day-old) and aged (21-day-old) fly heads with indicated genotypes. RNA levels were normalized to age-matched Ddrgk1 RNAi flies. Values represent average ± SD for 3 biological replicates. $^{*}p < 0.05$. **g** Immunoblots to visualize the level of ATP5A in young (3-day-old) and aged (21-day-old) heads of denoted genotypes. **h** Normalized ratio of ATP5A/β-actin indicated for representative lanes in (**g**). $^{*}p < 0.05$. **i–l** Survival curve of young flies of denoted genotypes fed with H_2O_2 to induce oxidative stress at 25 °C: **i** 5-day-old flies expressing UAS-RNAi transgene for Uba5 and Ufl1, $n \geq 160$, $p < 0.001$ (Log-rank test); **j** 3-day-old flies expressing Ddrgk1 RNAi under elav-Gal4, $n = 220$, $p < 0.001$; **k** Co-expression of Atg9 in Ddrgk1 knockdown flies (3-day-old), $n = 220$, $p < 0.001$; **l** flies in (**k**) reared on medium supplemented with 100 μM Rapamycin (Rapa), $n \geq 200$, $p < 0.001$

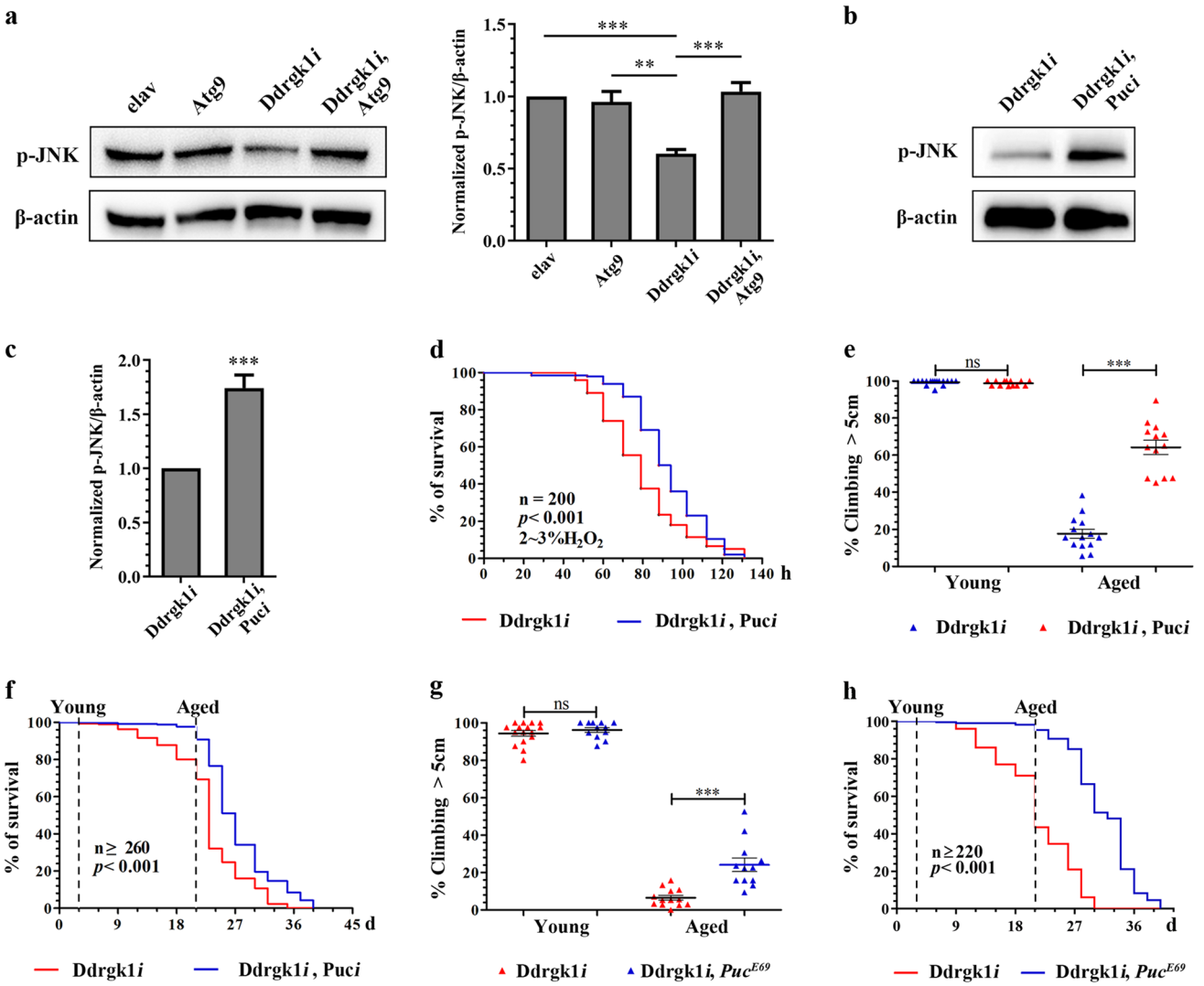

Fig. 7 JNK is involved in the neuroprotection of Ufmylation. **a** Immunoblot to detect JNK phosphorylation in heads of young flies (3-day-old) driven by elav-Gal4. Flies depleted Ddrgk1, or overexpressing Atg9, or both were treated with H_2O_2 at 25 °C for 60 h. Anti-β-actin was used as loading control. Right panel: histogram showing the normalized ratio of p-JNK/β-actin indicated for representative lanes in left panel. Data represent 3 independent experiments. $^{**}p<0.01$, $^{***}p<0.001$. **b** Immunoblot to detect JNK phosphorylation in heads of 3-day-old elav flies depleted Ddrgk1 with or without Puc RNAi. Flies were treated with H_2O_2 at 25 °C for 60 h. **c** Histogram showing the ratio of p-JNK/β-actin for representative lanes in (**b**). $^{***}p<0.001$ as per 3 repeats. **d** Survival curve on H_2O_2 of Ddrgk1 knockdown young flies (3-day-old) with or without Puc depletion by elav-Gal4. $n=200$; Log-rank test, $p<0.001$. **e** and **g** Climbing assays: **e** Ddrgk1 knockdown flies with or without Puc depletion; **g** Ddrgk1 knockdown by elav-Gal4 with one mutant copy of the *Puc* gene (Puc^{E69} as indicated). *ns* not significant, $^{***}p<0.001$. **f** and **h** Adult lifespan at 29 °C: **f** Ddrgk1 knockdown with or without Puc depletion, $n\geq260$, $p<0.001$; **h** Ddrgk1 knockdown flies heterozygous for Puc^{E69}, $n\geq220$, $p<0.001$. Broken lines indicate the time points when climbing assays were performed

the expression of most components of the Ufm1 pathway are modulated by ER stress [21, 23]. However, evidence consistently showed that deficiencies in Ufm1 resulted in aberrant accumulation of lysosomes and autophagy substrates in addition to increased cell apoptosis and vacuole formation in aged brain, all of which were ameliorated by introducing Atg9 into neurons without Ufmylation. These findings lend support to the notion that disturbance in the autophagic pathway is the primary cause of neurodegeneration associated with Ufm1 in *Drosophila*. In contrast, elevated UPR induced by ER stress was only detected in aged brains with Uba5 and Ufl1 abolished, but not in Ddrgk1-free counterpart, when compared to age-matched elav control (Supplemental Figure S2c–e), suggesting a case-to-case analysis perhaps is required in order to fully understand the role of Ufmylation in brain pathologies with age.

Actually a recent study has reported that knocking out Ddrgk1 in cultured MEF cells suppresses the

autophagosome-lysosome fusion with unknown mechanisms, leading to an impaired autophagic clearance and increased apoptosis [39]. In keeping with their conclusions, here we highlight the regulation of autophagy by Ufm1 modification through Atg9 in vivo in the aging neurons and thereby build a disease model in *Drosophila* potentially for degenerative disorders. Atg9 is a transmembrane protein essential for autophagosome formation and lysosome fusion. Our data demonstrate that Atg9 is a conserved substrate of Ufmylation and acts downstream of the Ufm1 machinery. Modification of Atg9 is likely to be mediated by the transient interaction between Atg9 and Ddrgk1 when Atg9 is synthesized and processed in the ER. Absence of Ddrgk1, the ER-anchoring protein in the Ufm1 E3 ligase, abrogates the Ufmylation of Atg9 and Atg9A respectively in *Drosophila* and MEF cells. Additionally in mammalian cells, we discover that Ddrgk1 is indispensable for the maintenance of endogenous Atg9A stability, further supporting the idea that Atg9 is functionally coupled to Ufm1 modification. Although an in depth exploration of Atg9 Ufmylation still awaits the identification and characterization of Ufmylated sites on Atg9, our findings so far propose a compelling mechanism through which the Ufm1 system regulates autophagic flux.

Using quantitative RT-PCR, we observed an age-dependent reduction in the mRNA levels of Patj and Tsc2 concurrent with a similar trend for Atg9 and Ufm1 components in *Drosophila* adult head (Fig. 1d). Since Atg9 is known to interact with Patj and Tsc2 to regulate intestinal cell growth by counteracting mTORC1 signaling [13], it is conceivable that repressing mTORC1 by its target 4EBP and S6K is able to improve the neuropathological changes caused by impaired Ufmylation in neurons. Nonetheless, given that mTORC1 is activated by sensing lysosomal amino acids on the surface of lysosome [50], the altered mTORC1 activity is also likely due to the raised number of acidified lysosomes as indicated by the LysoTracker probes. Indeed, lysosomal acidification previously has been implicated to be required for the degradative activity of hydrolases such as Cathepsins [51]. Moreover, expressions of Atg9 transgene only partly offset the increased lysosome vesicles caused by Ddrgk1 depletion (Figs. 2d and 4g), suggesting there perhaps is another way, through which Ufmylation regulates lysosome and subsequent mTORC1 independent of Atg9. Such a mechanism becomes plausible in particular when it explains why inhibiting mTORC1 by rapamycin in the presence of Atg9 could further prolong the survival of Ddrgk1-defective flies fed with H_2O_2. In fact, a motif of systematic regulation is also recommended in mammals as huge amounts of differentially expressed proteins have been identified to be enriched in lysosome- and autophagy-related pathways in Ddrgk1 deletion cells [39]. Many other *Drosophila* autophagy mutants, such as Atg5, Atg7, and Atg17, display reduced lifespan and decreased climbing activity likewise [52–54]. These observations, together with ours, imply that multiple targets probably are modified by Ufm1 and mediating neuroprotection, in concert with the Ufmylated substrates histone H4 and MRE11 during DNA damage response [25, 55, 56].

Despite the impairment of autophagy, disruption of Ufmylation reduces mitochondrial density through Atg9 in aged brains and phenocopies the mitochondrial defect reported before in indirect flight muscles of Atg9 knockdown flies [57]. Consistent with the mitochondrial abnormalities, young flies losing Ufm1 in neurons are hypersensitive to environmental oxidative toxicity. The JNK pathway is one of the mitogen-activated protein kinase (MAPK) cascades involved in stress responses including aging and oxidative stress [46]. Several studies have indicated that JNK is activated in degenerative disorders and the extent of JNK activity is correlated with the extent of cognitive decline [58]. However, our results suggest a beneficial effect of JNK signaling for Ufm1 flies in H_2O_2-triggered stress and age-progressive degeneration, which is in line with the protective function of JNK mediated by Atg9 in response to ROS stimulation as revealed by Tang and colleagues in both mammalian cells and *Drosophila* stem cells [59]. It has been emphasized that JNK activation may lead to the promotion of either cell survival or apoptosis, dependent on the magnitude and duration of stress exposure. Then it will be of interest to learn whether considering these issues will help to clarify the controversial role of JNK in the dynamic progression of degeneration in neurons.

Besides, Atg9 is also known to enable lipid mobilization from lipid droplets (LDs) to autophagosomes and mitochondria [60]. Morphological and functional dissection of early steps of autophagy has defined that the phagophore membrane is rich in phospholipids, the fatty acid (FA) precursors of which could be derived from hydrolysis of triglycerides stored in LDs. Cryo-electron microscopy analyses unveiled that Atg9 comprises a network of internal cavities proposed to participate in the delivery of phospholipids to expanding phagophores for progression of the autophagy process [61, 62]. Abrogation of Atg9A in human cells not only inhibited autophagy, but also resulted in increased number and size of LDs, as well as impaired transport of FAs from LDs to mitochondria and consequently reduced mitochondrial respiration [60]. Mechanistically, these literatures, together with our findings, established an intricate linkage between Atg9 and mitochondrial homeostasis, in which Ufmylated Atg9 may engage in key steps such as lipid mobilization. Apart from autophagy, Atg9 also influences the actin cytoskeleton and cell protrusion/neurite growth in *Drosophila* and human cells, pointing to a wider role of Atg9 in general vesicular trafficking driving cell migration [63, 64]. These other processes, likely affected by Atg9 levels in addition to mTORC1

and JNK signaling, could be pivotal for the stereotypic neuronal connectome in the brain, and worthy of study in future.

Materials and methods

Drosophila strains

Flies and crosses were raised at 25 °C, 70% humidity in an environmentally controlled incubator on a 12 h light–dark schedule unless otherwise indicated. *UAS-Atg9*^{RNAi} (28,055), *UAS-Patj* (39,735), *UAS-Patj*^{RNAi} (26,282 and 38,193), *UAS-S6K*^{RNAi} (42,572), *UAS-4EBP* (9147), *UAS-Puc*^{RNAi} (53,019), *UAS-GFP* (Chr2, 4775), and *UAS-GFP* (Chr3, 4776) were from Bloomington Stock Center. *UAS-Uba5*^{RNAi} (HMS01352), *UAS-Ufl1*^{RNAi} (HMJ30245), and *UAS-Ddrgk1*^{RNAi} (5862R-1) were from NIG-FLY. *UAS-Ddrgk1*^{RNAi} (110,238, KK library) and *UAS-Tsc1*^{RNAi} (22,252) were obtained from Vienna Drosophila RNAi center and *Puc*^{E69} (109,029) was from Kyoto Stock center. *UAS-GFP-Atg9* was described by Soukup et al. [65] and provided by Dr. Tong Chao at Zhejiang University. *UAS-Uba5*^{RNAi}, *UAS-Ufl1*^{RNAi}, *UAS-Ddrgk1*^{RNAi} (NIG), *UAS-Ddrgk1*^{RNAi} (KK), and *UAS-GFP-Atg9* were backcrossed 7 generations into the *w*^{1118} background to obtain isogenic lines, and other strains used were backcrossed at least 3 generations. Only male adults were utilized for phenotypic analysis.

Lifespan and climbing assay

Crosses were set up with 12 females per tube and flipped every day to prevent overcrowding. Groups of 20 males were collected within 24 h of eclosion and then aged at 29 °C on a 12 h light–dark schedule without further CO_2 exposure. Flies were flipped onto fresh food every 2–3 days and the number of dead flies was recorded. Climbing experiments were carried out at 3 to 6 pm for minimize circadian differences. Young (3-day-old) or aged (21- or 24-day-old) flies were transferred to clean cylindrical tubes measuring 2.5 × 9 cm with a line at the 5 cm marked, and allowed to rest for 30 min before the assay. Flies were tapped lightly down to the bottom of the tube, and the number that crossed the 5 cm mark in 30 s was counted. Tubes were placed horizontally and retested for another 30 min. The mean of the two technical replicates for each tube was recorded, and the percentage climbing was plotted as a single point. Each date point represents 12–20 files in one tube.

RNA isolation and quantitative real-time PCR

Total RNA was extracted from heads or brains of 35 adult male flies per sample as indicated, using Eastep Super Total RNA Extraction Kit (Promega, LS1040) according to the manufacturer's instructions. cDNA was prepared from 1 μg RNA using the HiScript II 1st Strand cDNA Synthesis Kit (Vazyme, R212). PCR was performed using Universal SYBR Green Supermix (BIO-RAD) and analyzed on Applied Biosystems QuantStudio 5 real-time PCR system. Results were normalized to *Kinesin* mRNA. The following primers were used: Kinesin, 5′-GCTGGACTTCGGTCGTAGAG-3′ and 5′-CTTTTCATAGCGTCGCTTCC-3′; S6K, 5′-GCAATATACTCGAGGCAGTCAAGC-3′ and 5′-CCGTCTGTCTGGAAGGCATAAAC-3′; Ddrgk1, 5′-GAAGCCAGCTCCTGATGAGATT-3′ and 5′-TCTACCAACACATCGCATCTAA-3′; Ufm1, 5′-ATGGAATTGGCATCAGCCCACAG-3′ and 5′-CTCGGATCCGTGCTTTAGGAACAC-3′; Uba5, 5′-ATGCTTACACGCTGCGGCATTG-3′ and 5′-TTGGCCAGCTCCACTTTGTCGTAG-3′; Ufc1, 5′-TGACGGCAAGACAGCGAAGATG-3′ and 5′-GCCCACAGTGGCTTAAAGTGATCC-3′; Ufl1, 5′-AGCATATTCGCGGCTCACTAAACG-3′ and 5′-CAGAACTTGCAGGCCAAATCGTG-3′; Atg9, 5′-TTGTCCAGATCCGAATCCTC-3′ and 5′-TCGTCTGGCTACTTGCCTTT-3′; Patj, 5′-AATTACAGCAGCAGCAGCAGAG-3′ and 5′-TTGGCACACTTTGTCCTAAACCTC-3′; Tsc2, 5′-GCATCGAATTGGCTAGAACGATTG-3′ and 5′-TGTTTAGGCCCTCAATTAGCTTCG-3′; Bip, 5′-TTCCTGCGTTGGTGTGTACAAG-3′ and 5′-TAGGAGGGAGTGATGCGGTTAC-3′; COXIII, 5′-CGAGATGTATCACGAGAAGG-3′ and 5′-GAATTCCGTGGAATCCTGTTG-3′; rp49, 5′-GCTAAGCTGTCGCACAAA-3′ and 5′-TCCGGTGGGCAGCATGTG-3′; Tsc1, 5′-TGACCTGGAGTCCAACATGACG-3′ and 5′-TTACCACCCACTGCTCCTTGTTC-3′; Puc, 5′-GGCCTACGACTTTATCGAAGATGC-3′ and 5′-AGAGCGACTTGTACCGCATGAC-3′; GFP, 5′-GCAGTGCTTCAGCCGCTA-3′ and 5′-AGCCTTCGGGCATGGC-3′.

Immunoblotting

Samples were boiled and resolved by SDS-PAGE before transferred to polyvinylidene fluoride membranes for antibody labeling. Protein bands were visualized using Tanon-3900 Chemiluminescence Imaging System and quantified by ImageJ. The following antibodies were used: anti-Ufm1 (Abcam, ab109305, 1:1000), anti-p62 (Abcam, BS6175, 1:1000), anti-eIF-2α (Bioworld, ab69090, 1:2000), anti-p-eIF-2α (Bioworld, ab69090, 1:2000), anti-V5 (Thermo Fisher, R96025, 1:5000), anti-Flag (Affinity, T0053, 1:5000), anti-LC3 (Affinity, AF5402, 1:2000), anti-ATP5A (Bioworld, BS3814, 1:1000), anti-GFP (Andes antibody Biotechnology, 01–0001, 1:10,000), anti-p-S6K (CST, 9209, 1:2000), and anti-p-JNK (CST, 4668, 1:2000). Anti-β-actin (Bioworld, AP0060, 1:10,000) or anti-H3 (Proteintech, 17,168-1-AP, 1:2000) was used as loading control. Image J was used for protein quantification.

TUNEL staining

Adult brains from aged male flies were dissected and fixed in PBS with 4% paraformaldehyde at room temperature for 30 min. After washing three times with PBS, samples were treated with proteinase K for 10 min and labeled for TUNEL assays using BrightRed Apoptosis Detection Kit (Vazyme, A113). Finally, brains were stained with DAPI for 10 min and imaged using a Leica SP8 confocal microscope. Confocal stacks from 10× objective were merged into a single plane using the maximum projection function for whole-brain imaging.

HE staining

For histology, aged male flies were fixed in 4% paraformaldehyde at room temperature for at least 24 h, followed by paraffin embedding and microtome sectioning. Serial 5 μm thick sections were prepared from fly heads and mounted on slides before hematoxylin and eosin staining to examine brain morphology using an Olympus microscope. Numbers of vacuoles greater than 2 μm in diameter were quantified by checking 4 serial sections at the level of the fan-shaped body.

LysoTracker staining

Brains from aged male adults were dissected in ice-cold Schneider medium and immediately incubated with LysoTracker Red (Beyotime, C1046) at a concentration of 100 μM for 35 min and DAPI for 10 min. Samples then were mounted on slides in this solution and imaged within 15 min of dissection on a Zeiss LSM 900 confocal microscope using a 40× objective. For each replicate within the experiment, one control and one mutant brain were imaged side by side, with identical microscope settings and photos taken from the same region of the sub-esophageal ganglion for each brain.

Oxidative stress assay

Young (3–5-day-old) male flies from indicated genotypes (20/vial) were grown at 25 °C on filter paper with 2–3% (vol/vol) H_2O_2 and 5% (wt/vol) sucrose to give oxidative stress. Rapamycin (MCE, AY-22989) was dissolved in 100% ethanol and then diluted to a final concentration of 100 μM with H_2O_2 and sucrose. The number of dead flies was counted every 4 h.

S2 cell culture and treatment

Drosophila S2 cells were maintained at 25 °C in Serum-Free Insect Cell Medium (Hyclone, SH30278.02) complemented with 10% Fetal Bovine Serum (Gibco, A3160801). For RNAi experiments, PCR primers for generating dsRNA against Ddrgk1, Ufl1 and Atg9 were designed as following: dsDdrgk1, 5′-GAATTAATACGACTCACTATAGGGAGAAACCTCCTGGCCGACTTCATT-3′ and 5′-GAATTAATACGACTCACTATAGGGAGAGAATTGTTTTGTTCTTGTTACTCTACCAACA-3′; dsUfl1, 5′-GGATTAATACGACTCACTATAGGGAGACGAACGAATATCTGCGGAGAA-3′ and 5′-GGATTAATACGACTCACTATAGGGAGACAAGGAAGCTGTTCTGCTTGTA-3′; dsAtg9, 5′-GGCTTAATACGACTCACTATAGGGAGATTTGGGCATAAGGCTTCTGA-3′ and 5′-TCGTTAATACGACTCACTATAGGGAGAGTTGCCATACGAAGATCACA-3′. dsRNAs were prepared using T7 RNAi Transcription Kit (Vazyme, TR102) and purified according to the manufacturer's instructions. S2 cells were treated with 37 nM dsRNA. For active mitochondria staining, cells were incubated in medium containing 100 nM cell permeant MitoTracker (Beyotime, C1035) for 35 min and DAPI for 10 min at 25 °C in a dark environment before imaged under a Leica SP8 confocal microscope.

TurboID

A V5 tag was added to a TurboID ligase derived from Flag-TurboID (addgene 124646) by PCR before the entire DNA fragment was cloned into pUAST-attB vector at EcoRI and XhoI sites for fly expression. Primers used for this step were: 5′-GATGAATTCATGAAAGACAATACTGTGCCTCTGAAG-3′ and 5′-CCTCTCGAGCTACGTAGAATCGAGACCGAGGAGAGGGTTAGGGATAGGCTTACCCTTTTCGGCAGACCGCAGA-3′. *Drosophila* Ddrgk1 was amplified from BDGP Gold cDNA GH18921 and further inserted into pUAST-attB-TurboID-V5 at EcoRI site to encode a Ddrgk1-TurboID-V5 fusion protein with 5′-TGGGAATTCATGGATCTGATCATTCTCGTGGGGATT-3′ and 5′-ATCGAATTCGGAGCTGGCTTCGCCGCC-3′. pActin-Gal4 was co-transfected with pUAST-Flag-Atg9 and TurboID constructs as indicated using Effectene (Qiagen, 301,425) to express Flag-Atg9 and TurboID ligases in S2 cells for 30 h. Cells were harvested after 2 h treatment of 50 μM biotin or water as a control, and lysed in 50 mM Tris pH7.5, 150 mM NaCl, 1% NP-40 containing protease inhibitor (Beyotime, ST505). Biotin-labeled proteins were pulled down by incubating cell lysates with Streptavidin C1 beads (Thermo Fisher, 65,001) overnight. Finally beads were washed five times and boiled for immunoblotting. pUAST-Flag-Atg9 was described by Tang et al. [59] and provided by Dr. Chen Guang-Chao from Taiwan. pActin-Gal4 was a gift from Dr. Cai Yu at TLL (Singapore).

CHX chase assay

Immortalized mouse embryonic fibroblast (MEF) cells were derived from the DDRGK1F/F:ROSA26-CreERT2 mice

and described by Cao et al.[39]. The MEFs were cultured in DMEM medium supplemented with 10% fetal bovine serum and 50 μg/mL penicillin/streptomycin at 37 °C with 5% CO_2. MEFs were treated with 2 μM 4-OHT (Sigma, 68,392-35-8) or ethanol (EtOH) for 4 days to induce DDRGK1 deletion or as a control. To test the stability of proteins, MEFs were treated with 50 μg/mL CHX (Sigma, A6185) for indicated time to inhibit protein synthesis after stimulated with 4-OHT or ethanol. The protein levels of endogenous Atg9A and Ddrgk1 were determined by anti-Ddrgk1 (Proteintech, 21,445-1-AP, 1:2000) and anti-Atg9A (Abcam, ab108338, 1:2000), and quantified by image J.

Immunoprecipitation

Heads of adult male flies or MEF cells were lysed in lysis buffer (50 mM Tris, 150 mM NaCl, 1% NP-40) with protease inhibitor for 30 min. Lysates were immuno-precipitated with IgG, GFP or V5 antibody overnight before incubated with Protein A/G PLUS-Agarose (Santa Cruz, sc-2003) beads for another 2 h at 4 °C. Full-length Atg9A cDNA was amplified from pECMV-Atg9a-m-FLAG (MiaoLing Plasmid Platform, P5915) and cloned into pcDNA3.1/V5-His B vector at EcoRI and NotI sites for mammalian expression. Primers used for this step were: 5′-GACGAATTCATGGCG CAGTTTGACACTGAA-3′ and 5′-CGCGCGGCCGCATAC CTTGTGCACCTGAGG-3′. After MEFs were induced with 4-OHT or ethanol for 48 h, pcDNA construct was transfected using Effectene to express Atg9A for another 48 h.

Statistical analysis

Statistical analysis used the Student's *t* test (for normally distributed data) and Log-rank test (for data of lifespan). All data are presented as average ± SD. $p < 0.05$ was considered to be significant.

Supplementary Information The online version contains supplementary material available at https://doi.org/10.1007/s00018-023-04778-9.

Acknowledgements We thank Dr. Tong Chao (Zhejiang University) for kindly providing *UAS-GFP-Atg9* flies. We also thank Dr. Chen Guang-Chao (National Taiwan University) and Dr. Chen Yawen for providing pUAST-Flag-Atg9 plasmid. We thank Dr. Cai Yu (Temasek Life Sciences laboratory, Singapore) for pActin-Gal4 plasmid.

Author contributions WZ designed the experiments. HL, ZY, ZN, YC, ZW, LH and JZ performed the experiments. HL, ZY, ZN, YC, YC, FM and ZW analyzed the data. WZ, ZY and YC wrote the manuscript.

Funding This work was supported by the National Natural Science Foundation of China (No. 31701229, 32270516 and 31970413), Senior Health Research Project of Jiangsu Provincial Health Commission (LKM2023010) and National Key R&D Program of China (2018YFC1200201).

Availability of data and materials No new datasets were generated during the current study.

Declarations

Conflict of interest The authors declare no competing interests.

Ethical approval and consent to participate Not applicable.

Consent for publication All authors read and approved the final manuscript.

References

1. Klionsky DJ et al (2016) Guidelines for the use and interpretation of assays for monitoring autophagy (3rd edition). Autophagy 12(1):1–222. https://doi.org/10.1080/15548627.2015.1100356
2. Lahiri V, Hawkins WD, Klionsky DJ (2019) Watch what you (Self-) eat: autophagic mechanisms that modulate metabolism. Cell Metab 29(4):803–826. https://doi.org/10.1016/j.cmet.2019.03.003
3. Li H, Yu Z, Zhang W (2020) Misfolded protein aggregation and altered cellular pathways in neurodegenerative diseases. STEMedicine 1(4):e63. https://doi.org/10.37175/stemedicine.v1i4.63
4. Xi Y, Dhaliwal JS, Ceizar M, Vaculik M, Kumar KL, Lagace DC (2016) Knockout of Atg5 delays the maturation and reduces the survival of adult-generated neurons in the hippocampus. Cell Death Dis 7:e2127. https://doi.org/10.1038/cddis.2015.406
5. Nowosad A, Besson A (2022) Lysosomes at the crossroads of cell metabolism, cell cycle, and stemness. Int J Mol Sci 23(4):2290. https://doi.org/10.3390/ijms23042290
6. Jin M, Klionsky DJ (2014) Regulation of autophagy: modulation of the size and number of autophagosomes. FEBS Lett 588(15):2457–2463. https://doi.org/10.1016/j.febslet.2014.06.015
7. Webber JL, Tooze SA (2010) New insights into the function of Atg9. FEBS Lett 584(7):1319–1326. https://doi.org/10.1016/j.febslet.2010.01.020
8. Mizushima N, Yoshimori T, Ohsumi Y (2011) The role of Atg proteins in autophagosome formation. Annu Rev Cell Dev Biol 27:107–132. https://doi.org/10.1146/annurev-cellbio-092910-154005
9. Yamamoto H, Kakuta S, Watanabe TM, Kitamura A, Sekito T, Kondo-Kakuta C, Ichikawa R, Kinjo M, Ohsumi Y (2012) Atg9 vesicles are an important membrane source during early steps of autophagosome formation. J Cell Biol 198(2):219–233. https://doi.org/10.1083/jcb.201202061
10. Mari M, Griffith J, Rieter E, Krishnappa L, Klionsky DJ, Reggiori F (2010) An Atg9-containing compartment that functions in the early steps of autophagosome biogenesis. J Cell Biol 190(6):1005–1022. https://doi.org/10.1083/jcb.200912089
11. Popovic D, Dikic I (2014) TBC1D5 and the AP2 complex regulate ATG9 trafficking and initiation of autophagy. EMBO Rep 15(4):392–401. https://doi.org/10.1002/embr.201337995
12. Tamura H, Shibata M, Koike M, Sasaki M, Uchiyama Y (2010) Atg9A protein, an autophagy-related membrane protein, is localized in the neurons of mouse brains. J Histochem Cytochem: Off J Histochem Soc 58(5):443–453. https://doi.org/10.1369/jhc.2010.955690
13. Wen JK, Wang YT, Chan CC, Hsieh CW, Liao HM, Hung CC, Chen GC (2017) Atg9 antagonizes TOR signaling to regulate intestinal cell growth and epithelial homeostasis in Drosophila. eLife. https://doi.org/10.7554/eLife.29338

14. Hietakangas V, Cohen SM (2009) Regulation of tissue growth through nutrient sensing. Annu Rev Genet 43:389–410. https://doi.org/10.1146/annurev-genet-102108-134815
15. Zhang W, Thompson BJ, Hietakangas V, Cohen SM (2011) MAPK/ERK signaling regulates insulin sensitivity to control glucose metabolism in Drosophila. PLoS Genet 7(12):e1002429. https://doi.org/10.1371/journal.pgen.1002429
16. Liu Y, Mattila J, Ventela S, Yadav L, Zhang W, Lamichane N, Sundstrom J, Kauko O, Grenman R, Varjosalo M, Westermarck J, Hietakangas V (2017) PWP1 mediates nutrient-dependent growth control through nucleolar regulation of ribosomal gene expression. Dev Cell 43(2):240–252.e245. https://doi.org/10.1016/j.devcel.2017.09.022
17. Ma T, Hoeffer CA, Capetillo-Zarate E, Yu F, Wong H, Lin MT, Tampellini D, Klann E, Blitzer RD, Gouras GK (2010) Dysregulation of the mTOR pathway mediates impairment of synaptic plasticity in a mouse model of Alzheimer's disease. PloS One 5(9):e12845. https://doi.org/10.1371/journal.pone.0012845
18. Martina JA, Chen Y, Gucek M, Puertollano R (2012) MTORC1 functions as a transcriptional regulator of autophagy by preventing nuclear transport of TFEB. Autophagy 8(6):903–914. https://doi.org/10.4161/auto.19653
19. Hosokawa N, Hara T, Kaizuka T, Kishi C, Takamura A, Miura Y, Iemura S, Natsume T, Takehana K, Yamada N, Guan JL, Oshiro N, Mizushima N (2009) Nutrient-dependent mTORC1 association with the ULK1-Atg13-FIP200 complex required for autophagy. Mol Biol Cell 20(7):1981–1991. https://doi.org/10.1091/mbc.E08-12-1248
20. Wei Y, Xu X (2016) UFMylation: a unique & fashionable modification for life. Genom Proteom Bioinform 14(3):140–146. https://doi.org/10.1016/j.gpb.2016.04.001
21. Gerakis Y, Quintero M, Li H, Hetz C (2019) The UFMylation system in proteostasis and beyond. Trends Cell Biol 29(12):974–986. https://doi.org/10.1016/j.tcb.2019.09.005
22. Cai Y, Singh N, Li H (2016) Essential role of Ufm1 conjugation in the hematopoietic system. Exp Hematol 44(6):442–446. https://doi.org/10.1016/j.exphem.2016.03.007
23. Walczak CP, Leto DE, Zhang L, Riepe C, Muller RY, DaRosa PA, Ingolia NT, Elias JE, Kopito RR (2019) Ribosomal protein RPL26 is the principal target of UFMylation. Proc Natl Acad Sci USA. https://doi.org/10.1073/pnas.1816202116
24. Yoo HM, Kang SH, Kim JY, Lee JE, Seong MW, Lee SW, Ka SH, Sou YS, Komatsu M, Tanaka K, Lee ST, Noh DY, Baek SH, Jeon YJ, Chung CH (2014) Modification of ASC1 by UFM1 is crucial for ERalpha transactivation and breast cancer development. Mol Cell 56(2):261–274. https://doi.org/10.1016/j.molcel.2014.08.007
25. Qin B, Yu J, Nowsheen S, Wang M, Tu X, Liu T, Li H, Wang L, Lou Z (2019) UFL1 promotes histone H4 Ufmylation and ATM activation. Nat Commun 10(1):1242. https://doi.org/10.1038/s41467-019-09175-0
26. Duan R, Shi Y, Yu L, Zhang G, Li J, Lin Y, Guo J, Wang J, Shen L, Jiang H, Wang G, Tang B (2016) UBA5 mutations cause a new form of autosomal recessive cerebellar ataxia. PloS One 11(2):e0149039. https://doi.org/10.1371/journal.pone.0149039
27. Liu J, Guan D, Dong M, Yang J, Wei H, Liang Q, Song L, Xu L, Bai J, Liu C, Mao J, Zhang Q, Zhou J, Wu X, Wang M, Cong YS (2020) UFMylation maintains tumour suppressor p53 stability by antagonizing its ubiquitination. Nat Cell Biol 22(9):1056–1063. https://doi.org/10.1038/s41556-020-0559-z
28. Verma P, Augustine GJ, Ammar MR, Tashiro A, Cohen SM (2015) A neuroprotective role for microRNA miR-1000 mediated by limiting glutamate excitotoxicity. Nat Neurosci 18(3):379–385. https://doi.org/10.1038/nn.3935
29. Cai Y, Pi W, Sivaprakasam S, Zhu X, Zhang M, Chen J, Makala L, Lu C, Wu J, Teng Y, Pace B, Tuan D, Singh N, Li H (2015) UFBP1, a key component of the Ufm1 conjugation system, is essential for ufmylation-mediated regulation of erythroid development. PLoS Genet 11(11):e1005643. https://doi.org/10.1371/journal.pgen.1005643
30. Chen F, Xing C, Zhang W, Li J, Hu T, Li L, Li H, Cai Y (2019) Salubrinal, a novel inhibitor of eIF-2alpha dephosphorylation, promotes erythropoiesis at early stage targeted by Ufmylation pathway. J Cell Physiol 234(10):18560–18570. https://doi.org/10.1002/jcp.28493
31. Zhu Y, Lei Q, Li D, Zhang Y, Jiang X, Hu Z, Xu G (2018) Proteomic and biochemical analyses reveal a novel mechanism for promoting protein ubiquitination and degradation by UFBP1, a key component of ufmylation. J Proteome Res 17(4):1509–1520. https://doi.org/10.1021/acs.jproteome.7b00843
32. Rubinsztein DC, Shpilka T, Elazar Z (2012) Mechanisms of autophagosome biogenesis. Curr Biol: CB 22(1):R29-34. https://doi.org/10.1016/j.cub.2011.11.034
33. Ravikumar B, Sarkar S, Davies JE, Futter M, Garcia-Arencibia M, Green-Thompson ZW, Jimenez-Sanchez M, Korolchuk VI, Lichtenberg M, Luo S, Massey DC, Menzies FM, Moreau K, Narayanan U, Renna M, Siddiqi FH, Underwood BR, Winslow AR, Rubinsztein DC (2010) Regulation of mammalian autophagy in physiology and pathophysiology. Physiol Rev 90(4):1383–1435. https://doi.org/10.1152/physrev.00030.2009
34. Bartlett BJ, Isakson P, Lewerenz J, Sanchez H, Kotzebue RW, Cumming RC, Harris GL, Nezis IP, Schubert DR, Simonsen A, Finley KD (2011) p62, Ref(2)P and ubiquitinated proteins are conserved markers of neuronal aging, aggregate formation and progressive autophagic defects. Autophagy 7(6):572–583. https://doi.org/10.4161/auto.7.6.14943
35. Branon TC, Bosch JA, Sanchez AD, Udeshi ND, Svinkina T, Carr SA, Feldman JL, Perrimon N, Ting AY (2018) Efficient proximity labeling in living cells and organisms with TurboID. Nat Biotechnol 36(9):880–887. https://doi.org/10.1038/nbt.4201
36. May DG, Scott KL, Campos AR, Roux KJ (2020) Comparative application of BioID and TurboID for protein-proximity biotinylation. Cells 9(5):1070. https://doi.org/10.3390/cells9051070
37. Cerami E, Gao J, Dogrusoz U, Gross BE, Sumer SO, Aksoy BA, Jacobsen A, Byrne CJ, Heuer ML, Larsson E, Antipin Y, Reva B, Goldberg AP, Sander C, Schultz N (2012) The cBio cancer genomics portal: an open platform for exploring multidimensional cancer genomics data. Cancer Discov 2(5):401–404. https://doi.org/10.1158/2159-8290.CD-12-0095
38. Gao J, Aksoy BA, Dogrusoz U, Dresdner G, Gross B, Sumer SO, Sun Y, Jacobsen A, Sinha R, Larsson E, Cerami E, Sander C, Schultz N (2013) Integrative analysis of complex cancer genomics and clinical profiles using the cBioPortal. Sci Signal 6(269):p11. https://doi.org/10.1126/scisignal.2004088
39. Cao Y, Li R, Shen M, Li C, Zou Y, Jiang Q, Liu S, Lu C, Li H, Liu H, Cai Y (2021) DDRGK1, a crucial player of Ufmylation system, is indispensable for autophagic degradation by regulating lysosomal function. Cell Death Dis 12(5):416. https://doi.org/10.1038/s41419-021-03694-9
40. Schleich S, Teleman AA (2009) Akt phosphorylates both Tsc1 and Tsc2 in Drosophila, but neither phosphorylation is required for normal animal growth. PloS one 4(7):e6305. https://doi.org/10.1371/journal.pone.0006305
41. Ziviani E, Tao RN, Whitworth AJ (2010) Drosophila parkin requires PINK1 for mitochondrial translocation and ubiquitinates mitofusin. Proc Natl Acad Sci USA 107(11):5018–5023. https://doi.org/10.1073/pnas.0913485107
42. Cisneros J, Belton TB, Shum GC, Molakal CG, Wong YC (2022) Mitochondria-lysosome contact site dynamics and misregulation in neurodegenerative diseases. Trends Neurosci 45(4):312–322. https://doi.org/10.1016/j.tins.2022.01.005
43. El Fissi N, Rojo M, Aouane A, Karatas E, Poliacikova G, David C, Royet J, Rival T (2018) Mitofusin gain and loss of function

drive pathogenesis in Drosophila models of CMT2A neuropathy. EMBO Rep. https://doi.org/10.15252/embr.201745241
44. Aparicio R, Rana A, Walker DW (2019) Upregulation of the autophagy adaptor p62/SQSTM1 prolongs health and lifespan in middle-aged Drosophila. Cell Rep 28(4):1029-1040.e1025. https://doi.org/10.1016/j.celrep.2019.06.070
45. Ramachandran A, Jaeschke H (2019) Acetaminophen hepatotoxicity. Semin Liver Dis 39(2):221–234. https://doi.org/10.1055/s-0039-1679919
46. Win S, Than TA, Kaplowitz N (2018) The regulation of JNK signaling pathways in cell death through the interplay with mitochondrial SAB and upstream post-translational effects. Int J Mol Sci 19(11):3657. https://doi.org/10.3390/ijms19113657
47. Biteau B, Karpac J, Hwangbo D, Jasper H (2011) Regulation of Drosophila lifespan by JNK signaling. Exp Gerontol 46(5):349–354. https://doi.org/10.1016/j.exger.2010.11.003
48. Martin-Blanco E, Gampel A, Ring J, Virdee K, Kirov N, Tolkovsky AM, Martinez-Arias A (1998) Puckered encodes a phosphatase that mediates a feedback loop regulating JNK activity during dorsal closure in Drosophila. Genes Dev 12(4):557–570. https://doi.org/10.1101/gad.12.4.557
49. Nalls MA et al (2014) Large-scale meta-analysis of genome-wide association data identifies six new risk loci for Parkinson's disease. Nat Genet 46(9):989–993. https://doi.org/10.1038/ng.3043
50. Kinghorn KJ, Gronke S, Castillo-Quan JI, Woodling NS, Li L, Sirka E, Gegg M, Mills K, Hardy J, Bjedov I, Partridge L (2016) A Drosophila model of neuronopathic gaucher disease demonstrates lysosomal-autophagic defects and altered mtor signalling and is functionally rescued by rapamycin. J Neurosci: Off J Soc Neurosci 36(46):11654–11670. https://doi.org/10.1523/JNEUROSCI.4527-15.2016
51. Senturk M, Lin G, Zuo Z, Mao D, Watson E, Mikos AG, Bellen HJ (2019) Ubiquilins regulate autophagic flux through mTOR signalling and lysosomal acidification. Nat Cell Biol 21(3):384–396. https://doi.org/10.1038/s41556-019-0281-x
52. Kim M, Sandford E, Gatica D, Qiu Y, Liu X, Zheng Y, Schulman BA, Xu J, Semple I, Ro SH, Kim B, Mavioglu RN, Tolun A, Jipa A, Takats S, Karpati M, Li JZ, Yapici Z, Juhasz G, Lee JH, Klionsky DJ, Burmeister M (2016) Mutation in ATG5 reduces autophagy and leads to ataxia with developmental delay. eLife. https://doi.org/10.7554/eLife.12245
53. Juhasz G, Erdi B, Sass M, Neufeld TP (2007) Atg7-dependent autophagy promotes neuronal health, stress tolerance, and longevity but is dispensable for metamorphosis in Drosophila. Genes Dev 21(23):3061–3066. https://doi.org/10.1101/gad.1600707
54. Kim M, Park HL, Park HW, Ro SH, Nam SG, Reed JM, Guan JL, Lee JH (2013) Drosophila Fip200 is an essential regulator of autophagy that attenuates both growth and aging. Autophagy 9(8):1201–1213. https://doi.org/10.4161/auto.24811
55. Cheng Y, Niu Z, Cai Y, Zhang W (2022) Emerging role of UFMylation in secretory cells involved in the endocrine system by maintaining ER proteostasis. Front Endocrinol 13:1085408. https://doi.org/10.3389/fendo.2022.1085408
56. Wang Z, Gong Y, Peng B, Shi R, Fan D, Zhao H, Zhu M, Zhang H, Lou Z, Zhou J, Zhu WG, Cong YS, Xu X (2019) MRE11 UFMylation promotes ATM activation. Nucleic Acids Res 47(8):4124–4135. https://doi.org/10.1093/nar/gkz110
57. Xu P, Damschroder D, Zhang M, Ryall KA, Adler PN, Saucerman JJ, Wessells RJ, Yan Z (2019) Atg2, Atg9 and Atg18 in mitochondrial integrity, cardiac function and healthspan in Drosophila. J Mol Cell Cardiol 127:116–124. https://doi.org/10.1016/j.yjmcc.2018.12.006
58. Stern M, McNew JA (2021) A transition to degeneration triggered by oxidative stress in degenerative disorders. Mol Psychiatry 26(3):736–746. https://doi.org/10.1038/s41380-020-00943-9
59. Tang HW, Liao HM, Peng WH, Lin HR, Chen CH, Chen GC (2013) Atg9 interacts with dTRAF2/TRAF6 to regulate oxidative stress-induced JNK activation and autophagy induction. Dev Cell 27(5):489–503. https://doi.org/10.1016/j.devcel.2013.10.017
60. Mailler E, Guardia CM, Bai X, Jarnik M, Williamson CD, Li Y, Maio N, Golden A, Bonifacino JS (2021) The autophagy protein ATG9A enables lipid mobilization from lipid droplets. Nat Commun 12(1):6750. https://doi.org/10.1038/s41467-021-26999-x
61. Matoba K, Kotani T, Tsutsumi A, Tsuji T, Mori T, Noshiro D, Sugita Y, Nomura N, Iwata S, Ohsumi Y, Fujimoto T, Nakatogawa H, Kikkawa M, Noda NN (2020) Atg9 is a lipid scramblase that mediates autophagosomal membrane expansion. Nat Struct Mol Biol 27(12):1185–1193. https://doi.org/10.1038/s41594-020-00518-w
62. Maeda S, Yamamoto H, Kinch LN, Garza CM, Takahashi S, Otomo C, Grishin NV, Forli S, Mizushima N, Otomo T (2020) Structure, lipid scrambling activity and role in autophagosome formation of ATG9A. Nat Struct Mol Biol 27(12):1194–1201. https://doi.org/10.1038/s41594-020-00520-2
63. Campisi D, Desrues L, Dembele KP, Mutel A, Parment R, Gandolfo P, Castel H, Morin F (2022) The core autophagy protein ATG9A controls dynamics of cell protrusions and directed migration. J Cell Biol. https://doi.org/10.1083/jcb.202106014
64. Kiss V, Jipa A, Varga K, Takats S, Maruzs T, Lorincz P, Simon-Vecsei Z, Szikora S, Foldi I, Bajusz C, Toth D, Vilmos P, Gaspar I, Ronchi P, Mihaly J, Juhasz G (2020) Drosophila Atg9 regulates the actin cytoskeleton via interactions with profilin and Ena. Cell Death Differ 27(5):1677–1692. https://doi.org/10.1038/s41418-019-0452-0
65. Soukup SF, Kuenen S, Vanhauwaert R, Manetsberger J, Hernandez-Diaz S, Swerts J, Schoovaerts N, Vilain S, Gounko NV, Vints K, Geens A, De Strooper B, Verstreken P (2016) A LRRK2-dependent EndophilinA phosphoswitch is critical for macroautophagy at presynaptic terminals. Neuron 92(4):829–844. https://doi.org/10.1016/j.neuron.2016.09.037